Check for updates

AGU ADVANCING EARTH AND SPACE SCIENCES

Water Resources Research

METHOD

10.1029/2024WR037370

iFLOW: A Framework and GUI to Quantify Effective Thermal Diffusivity and Advection in Permeable Materials From Temperature Time Series

A. Bertagnoli[1], C. Luce[2], R. van Kampen[3,4], U. Schneidewind[5], M. van Berkel[3], A. W. Tranmer[1], G. Vandersteen[6], S. Krause[5], and D. Tonina[1]

[1]Department of Civil and Environmental Engineering, Center for Ecohydraulics Research, University of Idaho, Boise, ID, USA, [2]US Forest Service, Rocky Mountain Research Station, Boise, ID, USA, [3]DIFFER - Dutch Institute for Fundamental Energy Research, Eindhoven, The Netherlands, [4]Department of Mechanical Engineering, Control Systems Technology Group, Eindhoven University of Technology, Eindhoven, The Netherlands, [5]School of Geography, Earth and Environmental Sciences, University of Birmingham, Birmingham, UK, [6]Department ELEC, Vrije Universiteit Brussel, Brussels, Belgium

Key Points:

- iFLOW is a novel framework for temperature time series analysis
- iFLOW helps users estimate advective flux and effective thermal diffusivity with their uncertainty
- The analysis is parsed into the mathematical model selection, signal processing, and parameter estimation steps

Supporting Information:

Supporting Information may be found in the online version of this article.

Correspondence to:

A. Bertagnoli and U. Schneidewind,
andrea.bertagnoli@outlook.com;
u.schneidewind@bham.ac.uk

Citation:

Bertagnoli, A., Luce, C., van Kampen, R., Schneidewind, U., van Berkel, M., Tranmer, A. W., et al. (2024). iFLOW: A framework and GUI to quantify effective thermal diffusivity and advection in permeable materials from temperature time series. *Water Resources Research*, *60*, e2024WR037370. https://doi.org/10.1029/2024WR037370

Received 28 FEB 2024
Accepted 3 NOV 2024

Abstract

iFLOW is a free, open-source, and python-based framework and graphical user interface to visualize and analyze temperature time series, and extract one dimensional thermal velocity, v_T, and bulk effective thermal diffusivity, k_e. Information of thermal properties of the sediment-water mixture (bulk) and water allows quantifying the one-dimensional Darcian flux, q, and seepage velocity, v, from v_T. Available software packages were developed to quantify q and k_e only based on a specific mathematical model or focused on specific data processing or parameter estimation techniques, and all these steps were lumped together preventing users to identify potential source of errors. iFLOW proposes a novel organizational philosophy with a modular framework that parses the analysis process into three fundamental steps: (a) the mathematical model, (b) signal processing, and (c) parameter estimation. iFLOW houses a suite of models and analysis techniques. This suite can be readily added to and expanded through its modular framework. iFLOW contains a wizard to guide users through the selection process with respect to the three fundamental steps. Users can analyze and visualize intermediate results to identify problematic issues in the time series data and improve data interpretation. Here, we present iFLOW and summarize its performance using a set of one-dimensional synthetic heat transport simulations.

Plain Language Summary

iFLOW is a free, open-source computer application to help users visualize and analyze temperature data. It calculates the water velocity within sediment along with thermal diffusivity from measured temperature data. Unlike other applications, iFLOW is flexible, allowing users to check for errors by breaking down the analysis into three parts: mathematical model selection, signal processing, and estimating parameters. It includes various models and methods that users can easily expand on. iFLOW also guides users through the analysis and in choosing options for these three analysis stages. We introduce iFLOW through a set of examples with simulated heat transport data.

1. Introduction

Water resources management in riverine environments can greatly benefit from mapping the temporal and spatial streambed seepage fluxes to inform water quantity, quality, and ecological functioning. These fluxes are critical at both hyporheic and river-aquifer scales (Krause et al., 2022; Tonina & Buffington, 2023), because they affect aquatic organisms (Baxter & Hauer, 2000; Boulton et al., 1998; Stuart, 1954; White & Hendricks, 2000), aquifer-river exchange (Conant, 2004; Constantz, 2008; Constantz & Stonestorm, 2003), and transport of solutes (Marzadri et al., 2014; Mulholland & DeAngelis, 2000), pollutants (Conant et al., 2004) and fine-sediment (Battin & Sengschmitt, 1999; Ren & Packman, 2007). Several field methods estimate streambed seepage fluxes (Buss et al., 2011; Hammett et al., 2022; Tonina, 2012) including pressure-gradient measurements (Baxter & Hauer, 2000; Bencala, 2005; Krause et al., 2012), solute tracers (Cox et al., 2007; Harvey et al., 2012; Zarnetske et al., 2008), synoptic discharge surveys (Woessner, 2020), seepage meters (Rosenberry et al., 2020), and temperature time-series measurements (Anibas et al., 2016; Constantz, 2008).

© 2024. The Author(s).
This is an open access article under the terms of the Creative Commons Attribution License, which permits use, distribution and reproduction in any medium, provided the original work is properly cited.

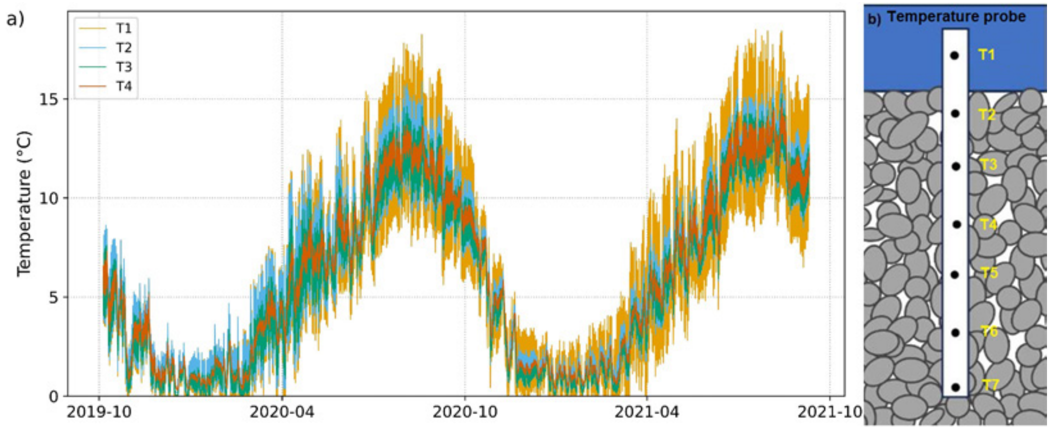

Figure 1. (a) Example of temperature time series collected at the water-sediment interface T1 and the first 3 sensors (T2, T3, and T4) within the streambed sediment vertically every 15 cm from November 2018 until July 2020 in Trails Creek (Idaho, USA) and (b) schematic of a temperature probe or temperature stake with seven temperature sensors (T1-T7).

Temperature-based methods, which use heat as a tracer, have become popular because of their affordability, robust measurement technology, negligible drift, and ability to collect long-term data (Bredehoeft & Papadopulos, 1965; Briggs et al., 2012; Goto et al., 2005; Hammett et al., 2022; Hatch et al., 2006; Keery et al., 2007; Luce et al., 2013; Schneidewind et al., 2016; Stallman, 1965; Vandersteen et al., 2015). Temperature sensors are housed in series within a PVC pipe, forming a probe or temperature stake, which is vertically driven into the sediment, and collect temperature time series at multiple vertical locations for short (few weeks) or long (several months or years) periods (Figure 1) (DeWeese et al., 2017; Schmidt et al., 2014).

Temperature-based methods estimate the vertical Darcian flux, q, by comparing temperature time series at different vertical locations by either (a) analyzing the temperature signals to extract the amplitude and phase of the temperature time series at one or multiple frequencies (e.g., Constantz & Thomas, 1996; Hatch et al., 2006; Keery et al., 2007; Luce et al., 2013; Stallman, 1965; van Kampen et al., 2022), or by (b) numerically (Anibas et al., 2018; e.g., McAliley et al., 2022; Voytek et al., 2014) or analytically (Lin et al., 2022) solving the heat transport equation. A less common approach treats transient temperature time series as a succession of steady states by applying steady-state solutions to temperature profiles at specific times or averaging them over periods (e.g., daily or weekly means) (Anibas et al., 2009; Irvine et al., 2020).

Several software packages facilitate the analysis of the temperature time series data and estimate q. These applications include *Ex-Stream* (Swanson & Cardenas, 2010), *VFLUX* (Gordon et al., 2012; Irvine et al., 2015), and *GW-SW Seepage Flux Spreadsheet* (Ford et al., 2021) for approach 1; and *1DTempPro* (Koch et al., 2016; Voytek et al., 2014), FLUX-BOT (Munz & Schmidt, 2017) and *tempest1d* (McAliley et al., 2022) for numerical and BDFLUX (Shi et al., 2024) for analytical approach 2. Approach 1, which estimate both the bulk effective thermal diffusivity, k_e, and vertical Darcian flux, q, is advantageous over approach 2, which requires to know k_e a-priori. Further, approach 1 has the additional benefit of computing the streambed elevation changes, Δz, under certain assumptions (DeWeese et al., 2017; Tonina et al., 2014). For these advantages, we focus on approach 1.

Current software packages do not separate the three steps of model selection, signal processing, and parameter estimation, limiting the identification of errors. This lumped approach affects the accuracy of parameter estimation and hinders problem identification. Additionally, they often do not provide information on model structure and parameter estimation uncertainty. These packages rely on proprietary platforms like MATLAB or Excel and are designed with specific solutions, limiting their flexibility and the scope of analysis.

To address these limitations, we propose iFLOW (Bertagnoli et al., 2024), a framework that separates the workflow into fundamental steps, guiding users through each step to allow intermediate results to be inspected and analyzed. iFLOW quantifies the signal-to-noise ratio (SNR) of the temperature time series and the uncertainty in parameter estimation. The framework includes mathematical approaches for steady-state and transient heat

19447973, 2024, 11, Downloaded from https://agupubs.onlinelibrary.wiley.com/doi/10.1029/2024WR037370 by National Forest Service Library, Wiley Online Library on [28/02/2025]. See the Terms and Conditions (https://onlinelibrary.wiley.com/terms-and-conditions) on Wiley Online Library for rules of use; OA articles are governed by the applicable Creative Commons License

transport and signal processing methods like Fast Fourier Transform (FFT) and local polynomial (LP). Here, we present the model, its validation with synthetic data and provide some operational guidelines.

2. Methods

Approach 1 solves the following simplified governing equation with different boundary conditions depending on the chosen mathematical model:

$$\frac{\partial T}{\partial t} = k_e \frac{\partial^2 T}{\partial z^2} - v_t \frac{dT}{dz} \tag{1}$$

The value of k_e and the thermal velocity, v_t, are quantified directly from analysis of the temperature time series and their solution does not require information on any thermal properties of the fluid and sediment (see Equation A2 in Supporting Information S1). The estimation of the Darcian flux, q, requires information on the fluid and sediment-water matrix properties such that $q = v_t \frac{\rho_m c_m}{\rho_w c_w} = v_t \gamma$, with $\gamma = \frac{\rho_m c_m}{\rho_w c_w}$, where ρ is the density and c the specific heat capacity with the subscripts m and w identifying the sediment-water matrix and water, respectively (see Supporting Information S1 for further details). The seepage velocity, v, of the water through the porous medium (the velocity within the pores) is quantified by dividing q by the porosity n, $v = q/n$.

Approach 1 relies on three steps: (a) mathematical model selection, for example, one dimensional with bounded or semi-infinite domain, (b) signal processing of the temperature time series, and (c) parameter estimation that quantifies the direction and magnitude of q and/or magnitude of k_e. Current software packages do not separate these three steps, such that users cannot properly identify the limitations of each step and/or locate potential sources of error in the time series, signal processing or parameter estimation. For instance, users may be unaware of some deficiencies in the signal processing step, such as spectral leakage (Pintelon et al., 2010; Rohling & Schuermann, 1983), or in the selection of the mathematical model, for example, effect of the lower boundary condition when choosing between a semi-infinite or bounded domain (e.g., van Kampen et al., 2022).

This lumped approach may affect the accuracy of the resultant parameter (q and k_e) estimation step and limit the ability to identify problems. Additionally, these software packages do not provide information on uncertainty of model structure or of parameter estimates.

Most existing software is generally designed for a specific solution. For example, *Ex-Stream* and *VFLUX* use the amplitude-based solution from Hatch et al. (2006) and only analyze the temperature signal frequency associated with daily stream water temperature fluctuations, the dominant frequency in natural streams. Because of the selected solutions, these software packages are limited to comparing signals at two vertical locations. Others, such as the *GW-SW Seepage Flux Spreadsheet* (Ford et al., 2021) were designed to only analyze temperature time series by breaking it up into short records of 24 hr such that analysis of long time series is labor-intensive because each day is analyzed separately. These limitations greatly constrain the information that can be used from the collected long temperature time series to predict q, k_e, and potentially Δz.

Heat transport in aquatic systems is complex, causing the quality and strength of the temperature signal to change over time (e.g., Figure 1a). For instance, rather steady temperature gradients may occur during the winter periods (e.g., January to March in Figure 1a) in streambeds of temperate and boreal climates, with colder temperature near the streambed surface and warmer temperatures deeper in the streambed (Figure 1). As days get longer, average stream water temperature and temperature amplitudes increase (e.g., March to July in Figure 1a). Superimposed to these seasonal and daily changes, temporal variations may occur over periods as short as a few hours due to storms (Barlow & Coupe, 2009) or tidal influences (Bianchin et al., 2010), or weekly due to cycles of cloudy and sunny days.

The propagation of the temperature signal within the streambed may then change temporally, such that a sensor placed deep in the streambed might only measure constant groundwater temperatures or seasonal variations. However, during summer, deep sensors can also capture high frequencies when the advective flux is strong enough to prevent these frequencies from being removed by diffusion and conduction.

Because of this complexity in the temperature signal, estimation of q and k_e from temperature time series may require different mathematical models (e.g., steady-state vs. transient or semi-infinite vs. bounded domain) or

19447973, 2024, 11, Downloaded from https://agupubs.onlinelibrary.wiley.com/doi/10.1029/2024WR037370 by National Forest Service Library, Wiley Online Library on [28/02/2025]. See the Terms and Conditions (https://onlinelibrary.wiley.com/terms-and-conditions) on Wiley Online Library for rules of use; OA articles are governed by the applicable Creative Commons License

10.1029/2024WR037370

19447973, 2024, 11, Downloaded from https://agupubs.onlinelibrary.wiley.com/doi/10.1029/2024WR037370 by National Forest Service Library, Wiley Online Library on [28/02/2025]. See the Terms and Conditions (https://onlinelibrary.wiley.com/terms-and-conditions) on Wiley Online Library for rules of use; OA articles are governed by the applicable Creative Commons License

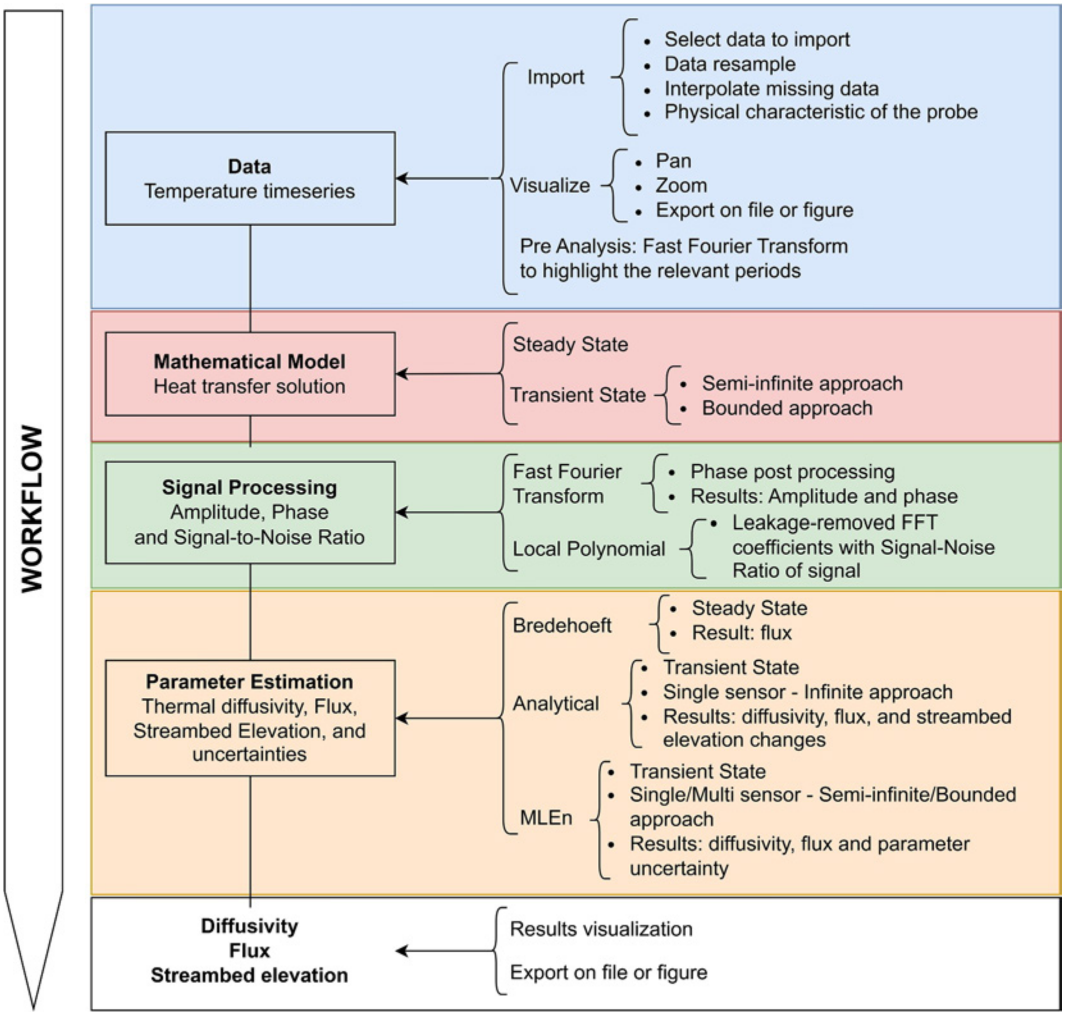

Figure 2. iFLOW modular framework separates the time series analysis into fundamental processing steps and presents the available modeling elements associated with each one.

different sensor locations depending on the quality of the temperature signal. Similarly, signal processing needs to be able to deal with changes in period and amplitude, and spectral leakage. Users need to be aware of when the signal at a bottom sensor is of poor quality to provide a proper boundary condition for the bounded domain or when the semi-infinite model may not be appropriate because the lower boundary does not satisfy the requirement of negligible thermal flux (van Kampen et al., 2022).

To address these limitations, we propose a novel organizational approach to the problem by explicitly parsing the workflow into its fundamental steps and by guiding users through each step to allow intermediate results to be inspected, analyzed, and interpreted (Figure 2). Further, our methodology quantifies the signal-to-noise ratio, SNR, of the temperature time series and the uncertainty in the parameter estimation for q and k_e to evaluate data quality. The iFLOW processing framework and graphical user interface, GUI, streamline and guide users to select the mathematical model, the signal processing method, and parameter estimator to quantify q and k_e from temperature time series collected at two or multiple vertical locations over a user-specified period (Figure 2).

The separation of the signal processing from the other steps provides users with tools to perform a processing step on amplitude and phase values extracted from the time series, as well as to correct or mitigate issues that arise prior to the parameter estimation step. This allows the user to (a) analyze and post-process the results at each step, (b) evaluate each source of error separately, and (c) add models separately to each component. The current version of iFLOW includes three mathematical approaches (thermal steady state (Bredehoeft & Papadopulos, 1965), and thermal transient state with a semi-infinite (e.g., Luce et al., 2013) and with bounded domains (van Kampen et al., 2022)) and two signal processing methods (Fast Fourier Transform, FFT, and local polynomial, LP (Pintelon et al., 2010; Vandersteen et al., 2015)). The framework includes two parameter estimation approaches (analytical solution of the semi-infinite domain and maximum likelihood estimator, MLE) based on single and multi-frequency analysis and for paired sensors and sensors at multiple vertical locations (Schneidewind et al., 2016). This flexibility allows users to employ either the FFT or LP to provide phase and amplitude estimates to the next parameter estimation step. Here, we show the capabilities and performance of iFLOW with a set of 1D synthetic heat transport simulations, supported by a top boundary time series signal that contained typical issues present in stream temperature time series, for example, change in amplitude and periods, trend in the temperature, no defined maximum or minimum and change in advection. The systematic application of the modeling framework under those conditions allows us to evaluate their implementation and to investigate the effect of window length based on the sampling rate and period, P_d, of the dominant frequency, which in natural streams is typically 24 hr.

3. iFLOW Graphical User Interface (GUI)

iFLOW is written in Python and uses commonly available libraries, for example, Numpy, Pandas and Matplotlib packages and is distributed as freeware and open source under a 2.0 Apache license. It is independent of the local operating system and its libraries are distributed under the GPL or MIT licenses, which avoids the use of proprietary software, such as Microsoft Excel or MATLAB, and licenses. iFLOW has a wizard to guide users through the whole process step-by-step, starting from the import of the raw temperature data, selection of the conceptual model, to exporting the results. Python is becoming the main coding language in geosciences, and we deliberately chose it because as all the code is open source, users can potentially add more signal processing methods, visualization options and parameter estimation models.

3.1. Data Import and Visualization

iFLOW allows users to visualize recorded temperature time series and fill in data gaps and temporally disaggregate the data using linear interpolation (Figure 3). Data can be retrieved from a single temperature probe with multiple vertical sensors or from multiple probes with different sensor sets. During visualization, users can process the time series to identify dominant and other significant frequencies of the temperature signals, exploring weekly, monthly, or other periodic behaviors. This helps in selecting the most appropriate mathematical model and signal processing method.

For instance, in temperate and boreal streams, the temperature signal may show a rather steady vertical gradient for weeks to months during winter. In such cases, the steady state method (Bredehoeft & Papadopulos, 1965) can be applied to quantify the flux when the thermal properties are known, whereas a transient method would be more appropriate in periods with temperature variations.

3.2. Mathematical Models

iFLOW incorporates three mathematical models: steady state, transient state with semi-infinite and bounded domains allowing the user to solve Equation 1. iFLOW uses the analytical solution proposed by Bredehoeft and Papadopulos (1965) for thermal steady state conditions (see Supporting Information S1 for details).

For the transient case, iFLOW guides users to select between a semi-infinite domain or bounded domain (see Supporting Information S1). The semi-infinite approach has a time-varying upper boundary condition specified with a temperature time series from a sensor typically at the water-sediment interface, whereas the lower boundary condition is set with a zero-temperature gradient. This is the model commonly used in available software packages (e.g., *Ex-Stream*, *VFLUX*, and *GW-SW Seepage Flux Spreadsheet*). Conversely the bounded approach uses temperature time series specified at both the upper and lower boundaries. It is crucial to ensure the quality of the lower boundary time series, for example, the signal-to-noise ratio should be >5 dB as suggested by van Kampen et al. (2022) because it strongly affects the solutions of the bounded model. iFLOW provides an estimate of the SNR (using the LP method) to evaluate the signal quality in the signal processing step.

Selection of the mathematical model also sets the minimum number of temperature signals that need to be collected and analyzed: the steady state requires three sensors (Bredehoeft & Papadopulos, 1965), the

19447973, 2024, 11, Downloaded from https://agupubs.onlinelibrary.wiley.com/doi/10.1029/2024WR037370 by National Forest Service Library, Wiley Online Library on [28/02/2025]. See the Terms and Conditions (https://onlinelibrary.wiley.com/terms-and-conditions) on Wiley Online Library for rules of use; OA articles are governed by the applicable Creative Commons License

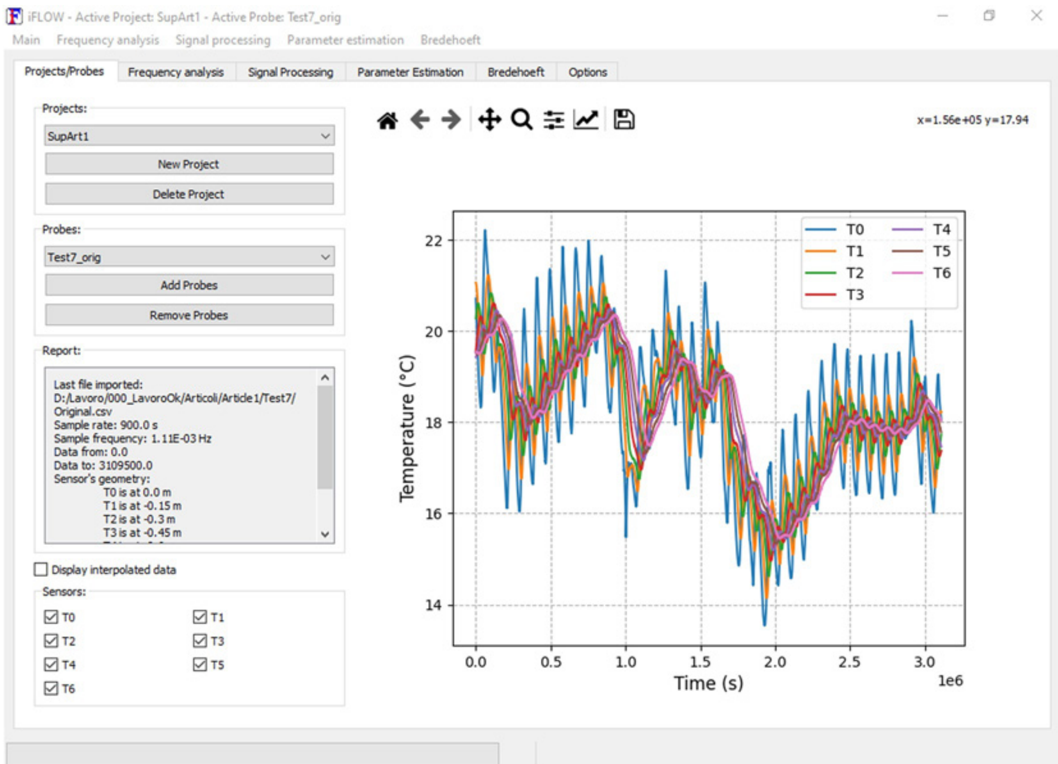

Figure 3. Example of the iFLOW environment showing the "Projects/Probes" tab of the Graphical User Interface, GUI. From this tab users can interact with the projects and the temperature probes related to a project; users can create or delete a project or create a new probe related to the active project following a step-by-step guided procedure.

semi-infinite analytical transient two sensors (Luce et al., 2013), the MLE semi-infinite domain at least two sensors (Schneidewind et al., 2016) and MLE finite domain at least three sensors (van Kampen et al., 2022).

3.3. Signal Processing

Once a model is selected, users can choose a signal processing method. At this stage, users may directly analyze and evaluate the results of the signal processing step. This analysis may help to identify potential issues in the extracted phase and amplitude. For example, during winter months high frequencies, for example, diel fluctuations, in the temperature time series may quickly fade with depth and may not be detected below a certain sensor. Thus, the user can change the lowest sensor to be used or increase the length of the moving window to analyze longer frequencies. It is important to note that increasing window length increases frequency resolution but reduces time resolution.

iFLOW includes two methods to extract the amplitude and phase from the temperature time series: the Fast Fourier Transform, FFT, and the local polynomial, LP method (Pintelon et al., 2010; Vandersteen et al., 2015). The FFT is a well-established and robust methodology but suffers from noise and spectral leakage issues (Harris, 1978; Schoukens et al., 2005). The LP method is specifically designed to minimize these issues that are naturally present in field-recorded temperature time series (Pintelon et al., 2010; Vandersteen et al., 2015).

Both methods can be applied to a fixed or moving window. The fixed window analyzes all the data or a user-specified subset to quantify a single set of phase and amplitude. It is a convenient selection when q is expected to be rather constant over time. Conversely, a moving window is more convenient for time-varying q because it has a finite length and moves through the data set with a step-size similar to the sampling rate. Users need to be aware of window length and its effect on distributing the system response within that window (DeWeese et al., 2017) and the trade off between frequency and time resolution. Users can specify the window length in iFLOW. Currently iFLOW uses a centered window (which could be modified to a forward or backward

19447973, 2024, 11, Downloaded from https://agupubs.onlinelibrary.wiley.com/doi/10.1029/2024WR037370 by National Forest Service Library, Wiley Online Library on [28/02/2025]. See the Terms and Conditions (https://onlinelibrary.wiley.com/terms-and-conditions) on Wiley Online Library for rules of use; OA articles are governed by the applicable Creative Commons License

10.1029/2024WR037370

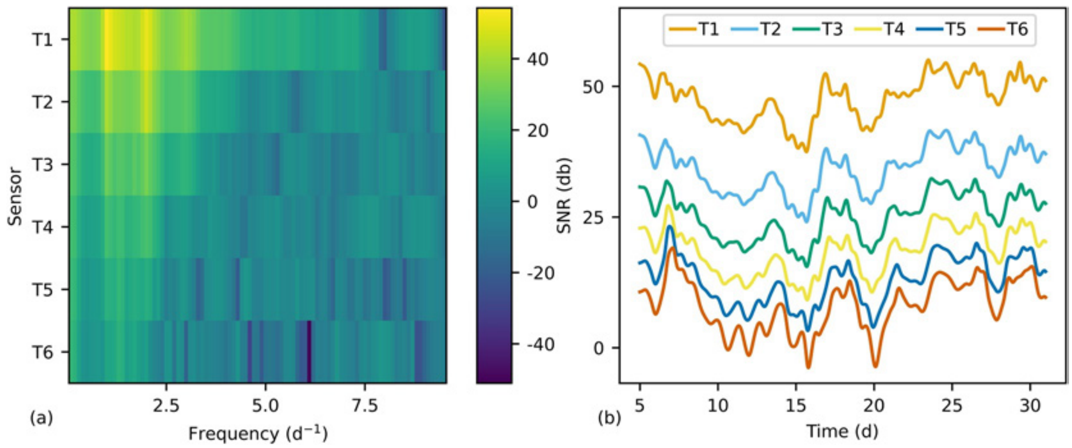

Figure 4. (a) Heatmap of the signal-to-noise ratio, SNR, for each sensor. This shows the SNR vertical trend within the sediment for each frequency extracted for a specific moving window. (b) SNR time trend of selected sensors and for one selected frequency.

window if needed) and thus, variations that take place over a period smaller than one window length are distributed within it.

The major issue of the FFT is the occurrence of spectral leakage, which occurs in case of non-periodic signals, signals with non-integer cycles of its periods, or time variations in parameters within the window length. When a temperature signal is non-periodic or has a finite-length with non-integer cycles of their periods, the temperature difference between the beginning and end of the window is an indicator of a non-periodic signal, which causes spectral leakage. The difference in temperature between the endpoints of the data window gives rise to high-frequency components, which are not present in the original signal. It looks as if energy at one frequency leaks into other frequencies, by increasing the energy of frequencies that may be present in the original signal or adding frequencies that are not present in the original signal. Spectral leakage can result in uncertainty regarding the values of the phase and amplitude extracted because of those added non-real frequencies and the "leakage" of energy to other frequencies, which are present in the signal.

To mitigate spectral leakage, iFLOW offers detrending and windowing functions, which are applied to the original signal before running the FFT (Harris, 1978; Schoukens et al., 2005). Detrending fits a linear trend to the temperature signal within the window and removes it, reducing the temperature difference between the window's endpoints. This is helpful when temperature signals have a cyclical period of temperature variations comparable with the window length. The windowing function technique multiplies the temperature signal within a window by a smooth, non-negative, bell-shaped function with a zero or near-zero value at each end of the windowing function. While this reduces spectral leakage, it can distort the signal, introducing systematic errors in phase estimation, though corrections are available for amplitude. Windowing functions also allow the FFT to handle non-integer cycles of the dominant period, such as 2.5 P_d instead of 2 or 3 P_d, by minimizing discontinuities between the start and end of the analyzed signal.

Conversely, the LP method does not require windowing functions or detrending. It acts as a non-linear form of detrending by extracting the trend directly from the frequency representation of the signal. It uses the coefficients extracted with the FFT, applies the LP method on the neighboring frequencies and compares it with a noiseless reference sensor to suppress the system and spectral leakage noise. Moreover, the LP method provides an estimate of the SNR that can be used as a quantitative metric for determining which sensors and frequencies have the best signal to be used in the subsequent parameter estimation step. Typically, sensors with an SNR <5 dB do not provide useable information and may be excluded from the analysis. iFLOW generates a heatmap of the SNR for each sensor, showing the SNR vertical trend within the sediment, the frequency extracted for a specific moving window, and a chart of SNR against time for a specific extracted frequency (Figure 4).

Signal processing methods like FFT constrain the phase between $\pm\pi$. However deep sensors may have phases much larger than $k\,\pi$ (with $k > 1$) (Figure 5a). iFLOW includes automated procedures to adjust the phase of a

19447973, 2024, 11, Downloaded from https://agupubs.onlinelibrary.wiley.com/doi/10.1029/2024WR037370 by National Forest Service Library, Wiley Online Library on [28/02/2025]. See the Terms and Conditions (https://onlinelibrary.wiley.com/terms-and-conditions) on Wiley Online Library for rules of use; OA articles are governed by the applicable Creative Commons License

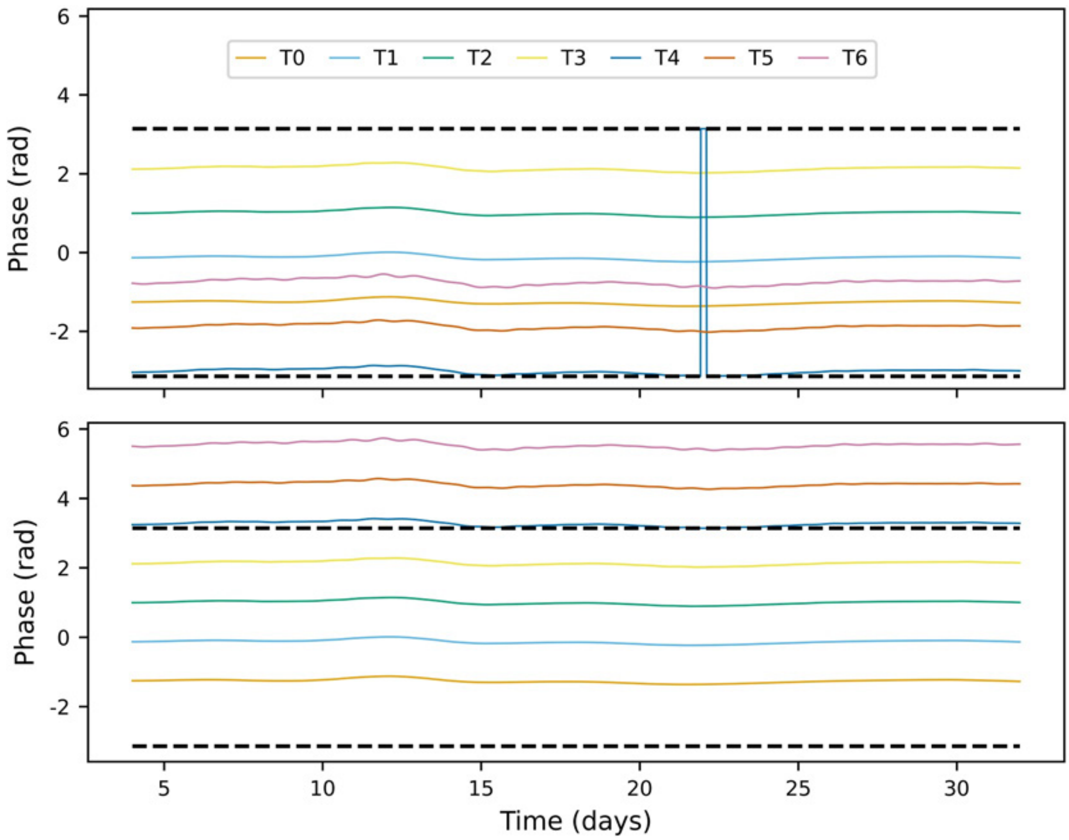

Figure 5. Example of ad-hoc phase correction. The top panel shows the phases extracted at each depth, T1 (top sensor) to T7 (bottom sensor) with the FFT with detrending and Hanning windowing function for the Test 7 (Table 1) and an 8-times the dominant period (192-hr) moving window length. The black dotted lines show $-\pi$ and $+\pi$ range, within which the phase is constrained by the FFT. However, the phase should increase linearly with depth, from the top to the bottom sensors, if the streambed substrate is homogeneous. iFLOW tools allow the user to manually shift the FFT-extracted phase by a given π amount.

selected frequency (period) to values larger than π when the signal arrival time to a sensor is longer than its period, for instance, when the temperature signal arrives to a lower sensor the following day for the 24-hr frequency. While the automated method addresses many cases, it may not correct all instances. Thus, iFLOW includes a tool to help users manually inspect and correct the extracted phases (Figure 5b). Users can also compare the results from FFT and LP methods to gain a better understanding of the processes and limitations.

3.4. Parameter Estimation

iFLOW estimates the fundamental parameters k_e and v_t from the temperature time series. Then, it quantifies q and v from user specified values of γ and n. Thus, uncertainty on q and v depends on v_t and on the thermal properties of the sediment and water and sediment porosity. For simplicity, we discuss q in the rest of the work because it is typically the quantity needed rather than thermal velocity.

3.4.1. Steady State

The steady-state parameter estimation step does not require signal processing. iFLOW includes a modified version of the approach proposed by Bredehoeft and Papadopulos (1965) to use n sensors within the top and bottom boundary conditions, instead of the original single sensor (see Supporting Information S1 for details). The unknown β parameter is estimated by minimizing the contribution from a system of n equations. The vertical flux q is then quantified by assigning parameter values for k_e, the density as well as the specific heat capacity of the water and the sediment-water mixture.

19447973, 2024, 11, Downloaded from https://agupubs.onlinelibrary.wiley.com/doi/10.1029/2024WR037370 by National Forest Service Library, Wiley Online Library on [28/02/2025]. See the Terms and Conditions (https://onlinelibrary.wiley.com/terms-and-conditions) on Wiley Online Library for rules of use; OA articles are governed by the applicable Creative Commons License

19447973, 2024, 11, Downloaded from https://agupubs.onlinelibrary.wiley.com/doi/10.1029/2024WR037370 by National Forest Service Library, Wiley Online Library on [28/02/2025]. See the Terms and Conditions (https://onlinelibrary.wiley.com/terms-and-conditions) on Wiley Online Library for rules of use; OA articles are governed by the applicable Creative Commons License

3.4.2. Transient State

iFLOW provides two options to estimate k_e and q for transient temperature time series. The first is the updated Stallman (1965) analytical approach proposed by Luce et al. (2013). This approach has the advantage that it can be used to estimate streambed thickness changes over time, Δz, once k_e has been quantified during a period with constant thickness between sensors (DeWeese et al., 2017). However, it is limited to the semi-infinite domain and to paired-sensor analysis. Multi-frequency analysis needs to be done individually for each frequency. Uncertainty, due to measurement set-up, can also be estimated (Luce et al., 2013).

The second option is the recently proposed Maximum Likelihood Estimation (MLEn) (van Kampen et al., 2022), which generalizes the previous methods presented by Schneidewind et al. (2016) and Vandersteen et al. (2015). The MLEn is applicable to both semi-infinite and bounded domains but is subject to a fixed geometry that does not account for potential change in streambed elevation (see Supporting Information S1 for details). However, it has several advantages over other methods: (a) use of multiple sensors at different vertical locations, (b) analysis of multiple frequencies from which it extracts information to estimate q and k_e, and (c) quantification of parameter as well as model structure uncertainty (van Kampen et al., 2022). The MLEn approach uses a transfer function in the complex domain using the two boundary conditions and one or more temperature measurement points in the vertical profile. The MLEn approach uses the Maximum Likelihood Estimator, which optimally takes uncertainty into account, to estimate the parameters by minimizing the cost function using a gradient descent algorithm. This algorithm requires starting values of q and k_e as seeding values. Users have two options to quantify the seeding value of q and k_e: (a) every-time option: the values are quantified at each time step with the analytical solution or (2) first-time option: the values are quantified with the analytical solution only at the first time step and then it uses the values quantified at the previous time step.

4. Simulations and Performance of iFLOW

iFLOW has a set of default values for the properties of the sediment and water and sediment porosity ($c_w = 4{,}183$ J/(Kg·°C); $c_s = 800$ J/(kg·°C); $\rho_w = 998$ kg/m^3; $\rho_s = 2{,}650$ kg/m^3; $n = 0.32$) (Table S1 in Supporting Information S1), which the user can change based on local measurements. We used those values for the simulations presented in this work.

4.1. Test Cases

We verify the performance of iFLOW by comparing iFLOW-estimated k_e and q to the effective thermal diffusivity 0.0432 m^2 d^{-1} (5×10^{-7} m^2 s^{-1}) and Darcian flux -0.3449 m d^{-1} (which corresponds to a vertical thermal velocity of -0.5184 m d^{-1} or -6×10^{-6} m s^{-1} and the negative sign indicates downwelling direction) imposed in a set of eight synthetic one dimensional (1D) numerical heat-transport models constrained by known top and bottom boundary conditions (Table 1). Each upper boundary time series (e.g., that of the sensor at the water-sediment interface which effectively measures stream water temperature) for test cases 1–6 is designed to have a selected problematic issue typically observed in temperature time series recorded in real world rivers. Test Case 7 uses a real temperature time series recorded in the streambed of a small gravel-bed river, Trail Creek near Ketchum (Idaho, USA), during 37 days in summer. Case 0 has a perfect sine signal and evaluates the performance of the models for the perfect case.

We used a sine wave to generate the basic temperature time-series at the upper boundary condition for all test cases except for test Case 7, which used real data from a creek in Idaho (Table 1). The basic sine wave has a 4°C amplitude, a constant mean temperature of 10°C, a 24 hr period, and data every 20 s. The fine temporal resolution was selected to meet the Currant requirements in numerically solving the one-dimensional numerical heat transport equation. Test 0 represents a basic sine wave, to which we applied a consistent white noise of 0.006°C. This is basically the reference case to verify that the model is well implemented. The next tests were used to quantify the behavior of the implemented models under different signal anomalies. Test cases 1–6 are variations of this basic wave signal and/or its propagation within the sediment (Table 1 and Figures S1–S7 in Supporting Information S1) representing changes in q mimicking natural temporal changes in fluxes (Test 1), random changes in amplitude due to changes in solar radiation magnitude (Test 2), random changes in period due to changes in solar radiation period (Test 3), changes in peak mimicking clouds and storms (Test 4), a sudden decrease in temperature mimicking a sudden arrival of cold water (Test 5), an increase in mean water temperature over several days as observed during spring (Test 6), and a real data set where many effects of tests 2–6 are present

10.1029/2024WR037370

Table 1
Upper Boundary Condition Temperature Time Series, T0, the for Eight Synthetic Test Cases

Test	Top boundary condition	Example
0	Consistent Sine wave.	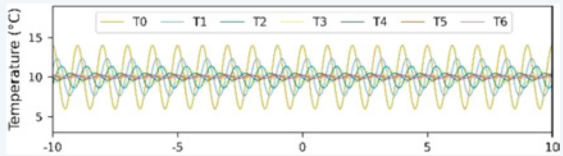
1	Sine wave with sudden thermal velocity increase to -0.6898 m d^{-1} (-12×10^{-6} m s^{-1}).	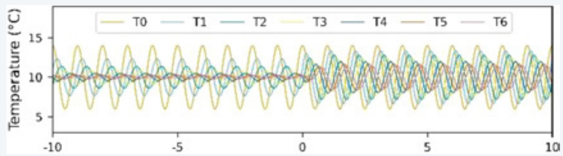
2	Sine wave, 10 days with random change in signal amplitude.	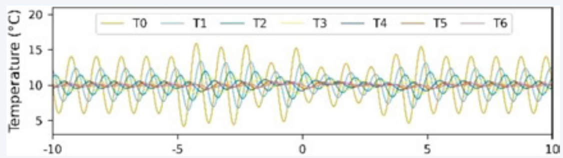
3	Sine wave, 10 days with random change in signal period.	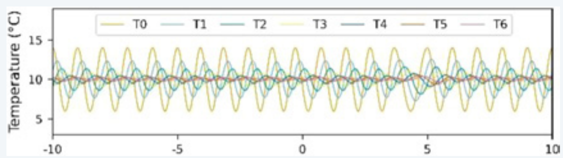
4	Sine wave, temperature maximum capped at 12 and 11°C on days 26 and 33, respectively.	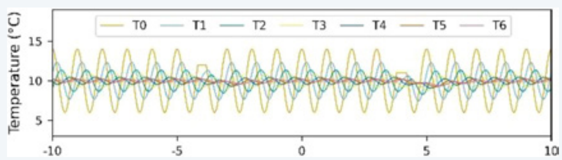
5	Sine wave with a sudden temperature decrease of 3°C.	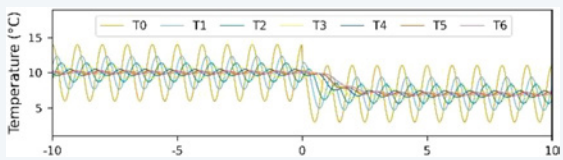
6	Sine wave, 10 days with linear increase in temperature of 0.018°C h^{-1}.	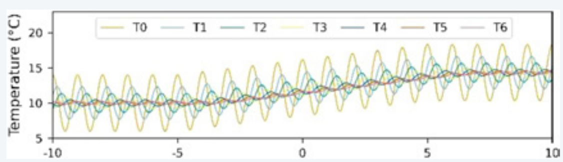
7	Real data recorded by a sensor located at the water-sediment interface in Trail Creek, Idaho.	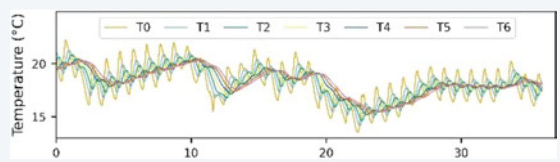

Note. Every time series, except for test 7, which is from a real gravel-bed stream, consists of a sine wave with an amplitude of 4°C and a period of 24 hr with a mean temperature of 10°C. The length of each test case is 60 days with a sample rate of 15 min. Solving the 1D advection-diffusion equation predicts the temperature time series at T1-T6 sensors within the sediment.

in the signal (Test 7). We used a slow vertical thermal velocity of -0.5184 m d^{-1} because those are more difficult to estimate with good accuracy than faster ones (Luce et al., 2013). To test the effect of faster velocity and sensor resolution we modified the simulations of Test 7 with slow (Test 7A) and fast (imposed $q = -0.864$ m d^{-1}) (Test 7B) velocity and sensor resolutions of 0.0625°C.

19447973, 2024, 11, Downloaded from https://agupubs.onlinelibrary.wiley.com/doi/10.1029/2024WR037370 by National Forest Service Library, Wiley Online Library on [28/02/2025]. See the Terms and Conditions (https://onlinelibrary.wiley.com/terms-and-conditions) on Wiley Online Library for rules of use; OA articles are governed by the applicable Creative Commons License

10.1029/2024WR037370

We numerically solved the 1D heat transport equation with finite difference techniques with first-order accuracy centered differences (Luce, Tonina, Applebee, et al., 2017; Luce, Tonina, & DeWeese, 2017). The time solution is explicit, and we set a 5 mm spatial step and 20 s time step to fulfill the Courant conditions for the stability of the numerical method with the imposed q and k_e. The selected temporal and spatial resolution provide negligible numerical errors for our cases. The model domain is a 5 m long homogenous system. The upper boundary condition is specified with the test time series (Table 1) while the lower boundary was set to a constant temperature of 10°C for all tests, representing a groundwater temperature common in temperate climate. The synthetic temperature time series within the domain were quantified every 20 s but we recorded it for further analysis in iFLOW every 5 min at virtual sensors with a vertical sensor spacing of 15 cm. We focused on the first seven sensors embedded into the sediment (T0-T6) such that the deepest sensor was located at 0.9 m below the surface.

4.2. iFLOW Performance

We adopted a moving window of eight times the dominant period length (8 P_d, 192 h) and a sampling rate of 15 min for both FFT and LP. We selected this sampling rate because it is a good compromise between adequate temporal resolution and storage requirements for year-long data collection. The chosen 8 P_d ensures solution convergence for the LP even in very complex heat transport cases and still preserve the temporal flux changes (Anibas et al., 2016). For the FFT approach, we used all the possible combinations of the FFT windowing function implemented in iFLOW, with and without the detrending correction. We used T0 at the water-sediment interface as the top boundary for all simulations and also as the reference sensor for LP, which was characterized with an order of the local polynomial with 2 and 8 degrees of freedom.

We analyzed all the available combinations of FFT windows and detrending options (on/off), to provide guidelines on which to use. We focused on the transient method for both semi-infinite and bounded domains, as well as MLEn and analytical solutions. To show the proper implementation of the models, we focus on three main models: the analytical model with FFT signal processing, FFT-analytical, and MLEn model with LP signal processing, using the semi-infinite domain, LP-MLEn$_{\mathrm{si}}$, and bounded domain, LP-MLEn$_{\mathrm{B}}$. However, users can mix-and-match methods as needed, for instance LP-analytical where the phase and amplitude are extracted by the local polynomial method and used in the analytical semi-infinite approach of Luce et al. (2013). We performed MLEn with both first-time and every-time options as described in Section 2.

We quantify the residuals, $Res_i = Var_{est,i} - Var_{imp,i}$, of each parameter, Var, for the ith simulation. The residuals of q and k_e were quantified over the entire temporal window by subtracting the imposed value (subscript imp) from the estimated (subscript est) the temperature time series with n points. We then quantify the model performance using the mean, M, the standard deviation, SD, the normalized root-mean-square error, $NRMSE$, by the imposed mean value, and the percent error, %E, of the residuals.

$$M = \sum \frac{Res_i}{n} \tag{2}$$

$$SD = \sqrt{\sum \frac{(Res_i - M)^2}{n-1}} \tag{3}$$

$$NRMSE = \frac{\sqrt{\sum \frac{Res_i^2}{n}}}{Var_{imp}}\% \tag{4}$$

$$\%_{error} = \frac{1}{n} \sum \frac{Res_i}{Var_{imp,i}}\% \tag{5}$$

4.3. Window Length and Sampling Rate

Window length has important effects on results including performance, resolution, and averaging of parameters within the window when q and k_e vary temporally within a window length. Here, we analyze the impact of the moving window length used in the LP and FFT signal processing step on the analytical and MLEn estimations of the parameters q and k_e, by comparing the results of four different window lengths for Test 7 (Table 1) and a 15-min sampling rate. We select the window lengths of four (96 h), six (144 h), eight (192 h), and ten (240 h) times

19447973, 2024, 11, Downloaded from https://agupubs.onlinelibrary.wiley.com/doi/10.1029/2024WR037370 by National Forest Service Library, Wiley Online Library on [28/02/2025]. See the Terms and Conditions (https://onlinelibrary.wiley.com/terms-and-conditions) on Wiley Online Library for rules of use; OA articles are governed by the applicable Creative Commons License

the period of the dominant frequency, P_d, which is 24 h in our case. The number of sample points within a window also has important implications for both FFT and LP signal processing because it impacts the number of frequencies that can be extracted. To provide guidelines on sampling rate and window length, we analyze the effect of sampling rate at 5, 10, 15, 30, and 60-min intervals for the window lengths of 1, 2, 4, 6, and 8 P_d (24, 48, 96, 144, and 192 h) for Test 7 (upper boundary defined with real data).

High-resolution data cannot always be collected in the field because of storage limitations, so long-term deployments sometimes use lower sampling frequencies. However, large time steps may lead to adopting long windows, which may reduce the precision and accuracy of capturing q and k_e variations in time. A potentially useful alternative is to disaggregate the data into shorter time steps, which increases the number of points within a window. Thus, we investigated the effect of linearly disaggregating the signal from 10, 15, 30, and 60 min to 5 min and compared their performance in supporting q and k_e estimation with those for the original 5 min time series. In these analyses, we used the Hanning windowing function with the detrending option for the FFT and MLEn with the first-time option.

5. Results and Discussion

5.1. FFT Windowing and Detrending

A comparison among the amplitudes and phases extracted for the available combinations of FFT windowing functions and detrending options shows that the rectangular window provides the lowest accuracy for phase extraction (Figure S9 in Supporting Information S1). Whereas the other combinations show comparable performance, the FFT Hanning windowing function performs, on average, better than the others among all the tests (M, SD and $\%_E$ for q and k_e show better performance for the Hanning and detrending option (Table S1 in Supporting Information S1 for Test 5). Consequently, we focus on results with this configuration in the remainder of the analysis of the iFLOW performance.

5.2. MLEn Starting Estimates

The MLEn performance is typically better with the first-time than every-time option with a moving window (Table S2 in Supporting Information S1). This is because fluxes typically change slowly in most natural riverine systems, so velocities are close to the previous value. Thus, the previous values for q and k_e are better starting points for solution convergence than the analytical estimates because the later may be impacted by localized issues in the signal, for example, subdued signal amplitude, sharp change in temperature (like for day 10–12 in Table 1, Test 7) and are based on the semi-infinite domain model with paired sensors. However, fluxes may change rapidly in streams impacted by hydropeaking, tides, or fast erosion and depositional processes. These changes may be large enough to create noticeable different values of q and k_e between the previous and the new time step. In this case, the every-time option, which sets the seeding value at each time step with the analytical values, may provide better convergence than the first-time option. Because of the better performance of the first-time option, we use this configuration for the MLEn model in the remainder of the analysis.

5.3. Test Performance

All models evaluated in iFLOW provided parameter estimates for q and k_e that closely match the imposed values with negligible differences (Table 2). FFT-analytical and LP-MLEn estimations provide comparable values, with LP-MLEn$_B$ typically superior when a disturbance occurs in the time series (Figure 6).

The sudden change in downwelling velocity imposed in Test 1 is properly detected by LP-MLEn as a sudden change but shifted by a half-window size in time (Figure 6b). The delay in the change of q is due to the LP signal processing that partially interprets the variation in the sensor signals as noise because it is not present in the reference sensor. Conversely, the FFT-analytical model smears the sudden change over an entire window length. The sudden change in velocity also impacts k_e, which exhibits a sudden change when the velocity changes for LP-MLEn that is not real (Figure 6a). As for q, the FFT-analytical solution detects an apparent but false change in k_e that persists over an entire window length.

Similarly, the models implemented in iFLOW predict k_e and q values very accurately when random changes in signal amplitude are imposed in Test 2 (Figures 6c and 6d). Errors for k_e and q spread over the entire disturbance period for the FFT-analytical model (Lautz, 2012) and are constrained within a short period in the LP-MLEn

19447973, 2024, 11, Downloaded from https://agupubs.onlinelibrary.wiley.com/doi/10.1029/2024WR037370 by National Forest Service Library, Wiley Online Library on [28/02/2025]. See the Terms and Conditions (https://onlinelibrary.wiley.com/terms-and-conditions) on Wiley Online Library for rules of use; OA articles are governed by the applicable Creative Commons License

19447973, 2024, 11, Downloaded from https://agupubs.onlinelibrary.wiley.com/doi/10.1029/2024WR037370 by National Forest Service Library, Wiley Online Library on [28/02/2025]. See the Terms and Conditions (https://onlinelibrary.wiley.com/terms-and-conditions) on Wiley Online Library for rules of use; OA articles are governed by the applicable Creative Commons License

Table 2
Mean, Standard Deviation, and Percent Error of the Thermal Diffusivity and Darcian Flux

		Diffusivity			Darcian flux		
Test case	Statistic	MLEn semi-infinite	MLEn bounded	Analytic	MLEn semi-infinite	MLEn bounded	Analytic
Test 0	M (m d^{-1})	0	0	0	0	0	-6.65×10^{-4}
	SD (m^2 d^{-1})	4.52×10^{-6}	3.01×10^{-6}	9.83×10^{-6}	3.79×10^{-6}	3.47×10^{-6}	1.14×10^{-4}
	$\%_E$ (%)	0.12	0.12	0.13	0.06	0.05	0.12
Test 1	M (m d^{-1})	-6.65×10^{-4}	-6.65×10^{-4}	3.33×10^{-3}	7.39×10^{-2}	7.39×10^{-2}	2.59×10^{-2}
	SD (m^2 d^{-1})	1.22×10^{-3}	1.31×10^{-3}	3.54×10^{-3}	9.56×10^{-2}	9.52×10^{-2}	4.02×10^{-2}
	$\%_E$ (%)	1.45	1.62	11.23	21.54	21.45	8.47
Test 2	M (m d^{-1})	0	0	0	0	0	0
	SD (m^2 d^{-1})	9.38×10^{-5}	5.49×10^{-5}	3.57×10^{-4}	1.39×10^{-3}	6.68×10^{-4}	4.78×10^{-3}
	$\%_E$ (%)	0.21	0.15	1.3	0.16	0.1	1.44
Test 3	M (m d^{-1})	0	0	0	0	0	-6.65×10^{-4}
	SD (m^2 d^{-1})	5.49×10^{-5}	4.28×10^{-5}	7.26×10^{-4}	4.87×10^{-4}	4.20×10^{-4}	5.58×10^{-3}
	$\%_E$ (%)	0.18	0.15	2.24	0.1	0.08	1.5
Test 4	M (m d^{-1})	0	0	0	0	0	-6.65×10^{-4}
	SD (m^2 d^{-1})	3.65×10^{-5}	2.62×10^{-5}	1.07×10^{-4}	5.98×10^{-4}	3.52×10^{-4}	1.37×10^{-3}
	$\%_E$ (%)	0.14	0.14	0.44	0.12	0.09	0.44
Test 5	M (m d^{-1})	0	0	0	5.32×10^{-3}	1.33×10^{-3}	-6.65×10^{-4}
	SD (m^2 d^{-1})	1.34×10^{-3}	5.18×10^{-4}	5.18×10^{-5}	1.45×10^{-2}	4.60×10^{-3}	4.17×10^{-4}
	$\%_E$ (%)	2.73	1.52	0.22	2.1	0.7	0.17
Test 6	M (m d^{-1})	0	0	0	0	0	-6.65×10^{-4}
	SD (m^2 d^{-1})	9.43×10^{-6}	9.43×10^{-6}	9.74×10^{-6}	1.08×10^{-4}	9.43×10^{-5}	1.05×10^{-4}
	$\%_E$ (%)	0.08	0.07	0.1	0.05	0.05	0.11
Test 7	M (m d^{-1})	0	0	0	-6.65×10^{-4}	-1.33×10^{-3}	-2.66×10^{-3}
	SD (m^2 d^{-1})	1.23×10^{-4}	1.12×10^{-4}	4.40×10^{-4}	1.34×10^{-3}	1.28×10^{-3}	6.77×10^{-3}
	$\%_E$ (%)	0.51	0.45	1.87	0.45	0.52	2.29
Test 7A	M (m d^{-1})	3.57×10^{-4}	3.94×10^{-4}	7.82×10^{-4}	1.25×10^{-3}	3.24×10^{-4}	-8.77×10^{-4}
	SD (m^2 d^{-1})	2.54×10^{-4}	3.93×10^{-4}	5.62×10^{-4}	3.27×10^{-3}	3.28×10^{-3}	9.67×10^{-3}
	$\%_E$ (%)	0.83	0.91	1.81	−0.36	−0.09	0.25
Test 7B	M (m d^{-1})	2.57×10^{-4}	2.14×10^{-4}	1.29×10^{-3}	-1.76×10^{-3}	-1.72×10^{-3}	-1.44×10^{-3}
	SD (m^2 d^{-1})	2.03×10^{-4}	1.70E $\times 10^{-4}$	1.08×10^{-3}	2.64×10^{-3}	2.48×10^{-3}	1.62×10^{-2}
	$\%_E$ (%)	0.59	0.49	3.00	0.31	0.30	0.25

Note. Estimation was performed using the MLEn and a moving window of 192 h. The ”first-time” option was chosen for estimating the starting values for the parameters. For comparison we also show estimation results when using the analytical approach, with the “Detrending” option activated and a Hanning FFT window.

model. The LP-MLEn$_B$ shows noticeably smaller errors than LP-MLEn$_{SI}$. The use of a local lower boundary better constrains the physical problem than the semi-infinite option because it has the memory of the signal at earlier times, which influences the heat transport through the soil.

All models perform well in Test 3, with LP-MLEn outperforming the FFT-analytical solutions in suppressing signal leakage due to period changes (Figures 6e and 6f). Similar to Test 2, the LP-MLEn$_B$ achieves better results than LP-MLEn$_{SI}$ with this signal perturbation. Capping the amplitude of the top signal (Test 4) has limited effects on the studied models (Figures 6g and 6h) because signal processing can isolate the phase and amplitude from the rest of the signal. Thus, localized impacts, like a cloudy day, have limited effect on this methodology.

All model performance for Test 5 is similar to the previous tests, especially Test 2, with the LP-MLEn$_{SI}$ having a sudden larger error than the others (Figures 6i and 6j). This is potentially due to the use of the reference signal as the top signal, which has a disturbance in it. All models exactly predict the imposed values with the presence of

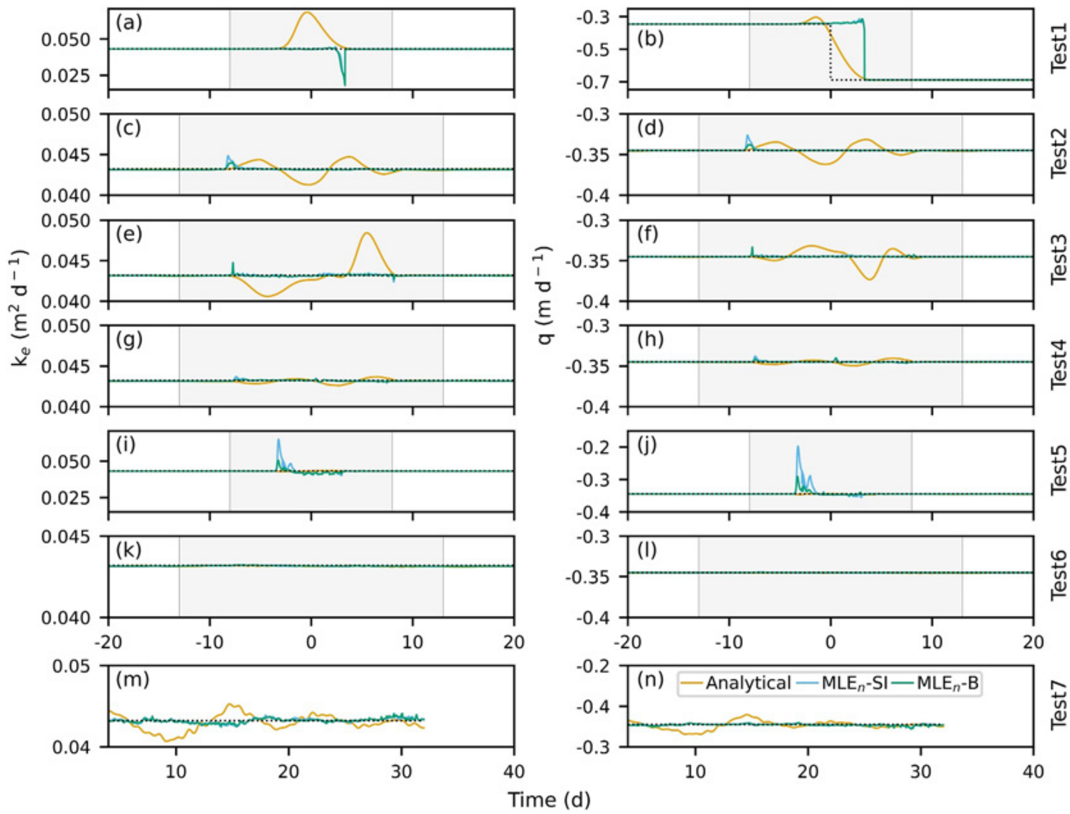

Figure 6. Estimated effective thermal diffusivity k_e (left panels) and Darcian flux q (right panels, positive and negative signs indicates upwelling and downwelling directions, respectively) around the time when the disturbance is applied for Test 1 (top panel) to Test 7 (bottom panel) with an 8-P (192 h) moving window length. The FFT-analytical model has the detrending option and Hanning windowing function active whereas the LP-MLEn model has first-time option active. The black dotted lines are the imposed values. The gray area represents the interval during which the moving window interacts with the imposed disturbance. Note that the vertical scales are not constant for each case. See Supporting Information S1 for graphs for the full study period.

temporal temperature gradients (Figures 6k and 6l), regardless of the model (Test 6) (Table 2 and Supporting Information S1). iFLOW performs quite well in Test 7, where all the previous effects are present in the field-recorded temperature time series applied as the upper boundary condition. The advantage of the LP-MLEn over the FFT-analytical model is noticeable, as it has very small errors through the entire time domain (Figures 6m and 6n).

The tests 7A and B performed as expected on the effects of flux magnitude and sensor resolution. Large q values generally reduce the error, especially for the LP-MLEn (Table 2, Test 7A vs. 7B). Conversely, decreasing the temperature sensor resolution from very high to 0.06°C negligibly increases the error (Table 2, compare 7B). These trends also hold for shorter window lengths of 96 hr (Table S3 in Supporting Information S1).

5.4. Window Length and Sampling Rate

During the signal processing step, shorter window lengths (e.g., 2–4 P_d) lead to greater variations in phases and amplitudes compared to longer window lengths (e.g., 8–10 P_d) (Figure S11 and Table S4 in Supporting Information S1). These variations, errors linked to signal processing and data limitations to describe the complexity of a signal, increase with decreasing window length and affect the parameter estimates of q and k_e (Figure 7). While window lengths of 6 P_d (144 h) or longer have similarly high accuracy, shorter window lengths have the advantage of better detecting real temporal changes of q and k_e. This is particularly important for systems where q and k_e change over time spans similar to P_d. Shorter window lengths are more effective at detecting natural variations caused by hydromorphological (in-stream bedform-flow interaction) and hydrologic (water table and

19447973, 2024, 11, Downloaded from https://agupubs.onlinelibrary.wiley.com/doi/10.1029/2024WR037370 by National Forest Service Library, Wiley Online Library on [28/02/2025]. See the Terms and Conditions (https://onlinelibrary.wiley.com/terms-and-conditions) on Wiley Online Library for rules of use; OA articles are governed by the applicable Creative Commons License

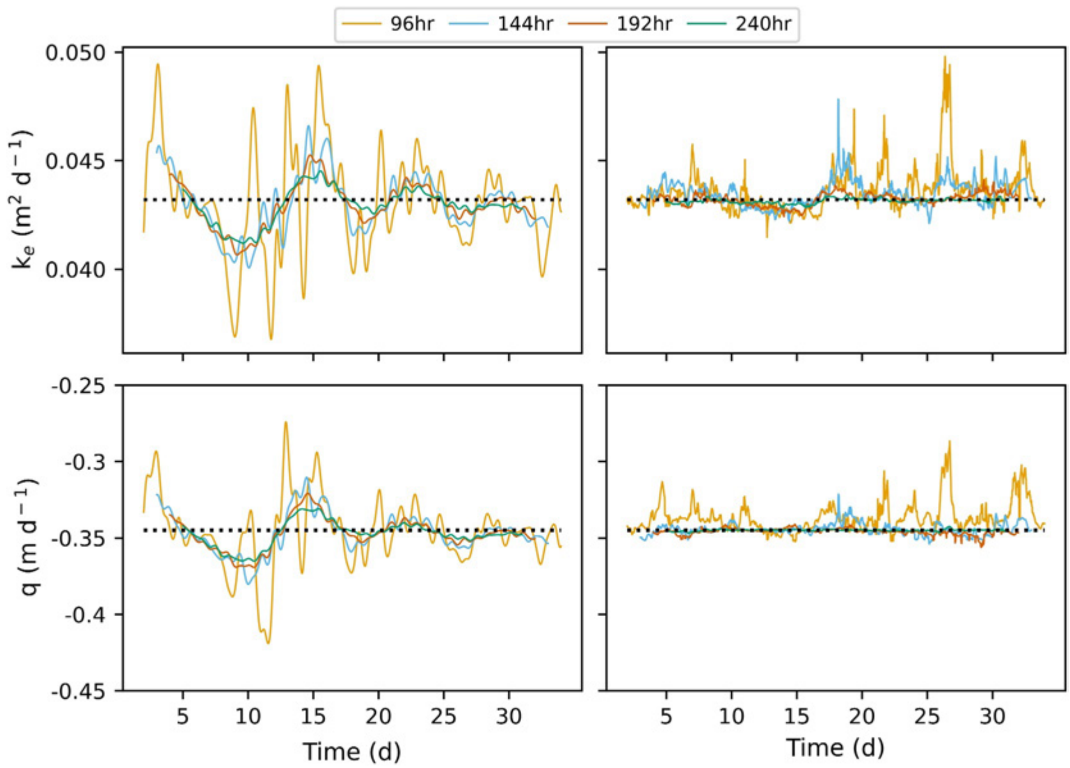

Figure 7. Estimated k_e (Top panels) and q (bottom panels) for Test 7 with the FFT-analytical approach with Hanning and detrending (left panels) and LP-MLEn$_{SI}$ (T0 as reference and first-time option) for four window length of 4, 6, 8, and 10 P_d. The black dotted line indicates the imposed values.

stream stage) changes. However, short windows have the disadvantage that signal processing may be impacted by local noise and anomalies in the temperature signal, which may lead to unrealistic and potentially spurious estimates of q and k_e. Larger window sizes mitigate these issues but may compromise the detection of temporal variations. Therefore, the choice of window size should be carefully evaluated based on system dynamics. For instance, Vandersteen et al. (2015) used moving window lengths of 3, 10 and 20 P_d (with $P_d = 24$ h) on a 90-day data set with 10 min resolution, finding that shorter windows increased temporal variability of q. Conversely, Anibas et al. (2016) used a 10 P_d window length for a 158-day data set with 10 min resolutions, because shorter window lengths resulted in poor SNR.

Changing the window length affects signal processing because it alters the number of data points analyzed and the available frequencies. Shorter window lengths typically increase the signal-to-noise ratio, leading to higher errors in q, regardless of the model or sampling rate (Figures 8a–8c). However, errors remain small (NRMS <10%) and similar for window lengths greater than 4 P_d (96 h). Sampling rates, within those typically used in the field, become noticeably important when decreasing the window lengths shorter than 4 P_d, because they affect the ability to determine phases and amplitudes and their uncertainties. For instance, the FFT-analytical model can find a solution for 2 P_d and 1 P_d window lengths only with a 5-min sampling rate, less frequent sampling limits solutions to a few moving windows in the entire time series. Whereas FFT-analytical does not show a clear threshold of the minimum number of points necessary within a window length, our analysis suggest that the LP method requires about 193 data points within a moving window to compute the transient to detrend the signal. As the MLEn requires variance estimates of the Fourier coefficients, the minimum number of data points required is about 195 to provide a solution for the case analyzed here for both semi-infinite and bounded domains. These values depend on the quality and characteristics of the forcing signal.

Disaggregating data into finer time steps can increase the number of data points, aiding signal processing techniques (Figure 8d). This approach is useful when data are originally collected every 10 or 15 min, which would require a 4 P_d window length (Figures 8a–8c). Although disaggregation does not add new information, it

19447973, 2024, 11, Downloaded from https://agupubs.onlinelibrary.wiley.com/doi/10.1029/2024WR037370 by National Forest Service Library, Wiley Online Library on [28/02/2025]. See the Terms and Conditions (https://onlinelibrary.wiley.com/terms-and-conditions) on Wiley Online Library for rules of use; OA articles are governed by the applicable Creative Commons License

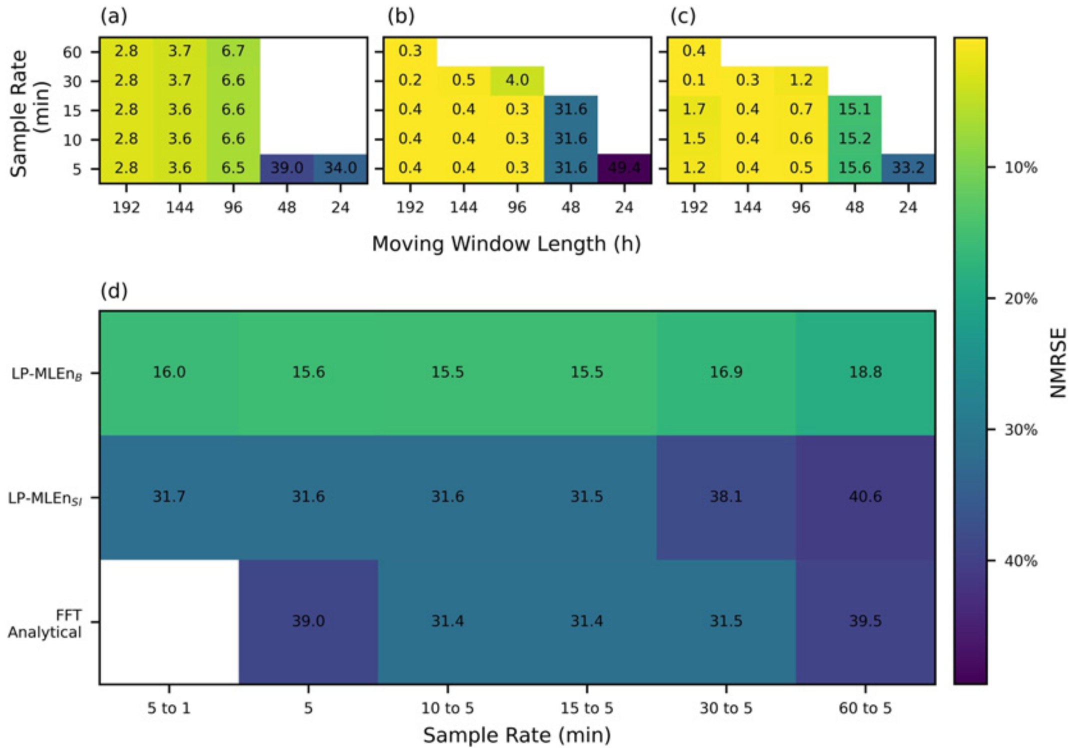

Figure 8. Heat maps of *NRMSE* of q for the FFT-analytical (a), LP-MLEn semi-infinite, LP-MLEn$_{SI}$ (b) and LP-MLEn bounded, LP-MLEn$_B$ (c) for a combination of sampling rate and window length. Panel (d) shows the heatmap *NRMSE* for linearly disaggregating the temperature time series from 60 (60–5), 30 (30–5), 15 (15–5) and 10 (10–5) minutes to 5 min along with those for the native 5 (5 min) minutes case with a 2-P (48 h) window. White color cells in (a–c) indicates that the model did not find a solution. Black numbers in the cell represent the normalized error.

can enhance numerical signal processing, particularly for the LP method used to estimate phases and amplitudes. Disaggregation to 5 min time steps from 10 or 15 min shows similar errors (NRMSE) compared to the 5 min original case (compare 5 with 10-to-5 and 15-to-5, Figure 8b), whereas larger errors occur when disaggregating from 30 or 60 min.

iFLOW provides several options for temperature time series analysis that help users better understand the hydrological processes involved in heat transport in streambeds and other saturated porous media, which sets it apart from others available software packages (Ford et al., 2021; Gordon et al., 2012; Irvine et al., 2015; Swanson & Cardenas, 2010). Its application can go beyond temperature time series analysis and include any transient data set. Besides temperature analysis, iFLOW can handle any transient data set, such as interpreting time series of electrical conductivity due to natural or anthropogenic (salt injections) processes. The choice of Python, a common language used in geoscience, coupled with iFLOW's open access and modular framework allow users to expand data visualization and analysis, including signal processing and parameter estimation techniques. For instance, an extension we are considering is adding a particle swarm algorithm to improve parameter estimation beyond the currently used gradient descent algorithm in MLEn.

6. Conclusion

We present iFLOW (Bertagnoli et al., 2024), a novel framework and GUI for analyzing temperature time series data. It estimates the effective thermal diffusivity, k_e, of the sediment-water matrix and one-dimensional thermal velocity from which the vertical Darcian flux, q and the seepage velocity, v, can be calculated using information on the thermal properties of the sediment and water as well as sediment porosity.

iFLOW's workflow helps break down the analysis into three parts: mathematical model selection, signal processing, and parameter estimation. This approach allows users to review intermediate results and understand or

19447973, 2024, 11, Downloaded from https://agupubs.onlinelibrary.wiley.com/doi/10.1029/2024WR037370 by National Forest Service Library, Wiley Online Library on [28/02/2025]. See the Terms and Conditions (https://onlinelibrary.wiley.com/terms-and-conditions) on Wiley Online Library for rules of use; OA articles are governed by the applicable Creative Commons License

19447973, 2024, 11, Downloaded from https://agupubs.onlinelibrary.wiley.com/doi/10.1029/2024WR037370 by National Forest Service Library, Wiley Online Library on [28/02/2025]. See the Terms and Conditions (https://onlinelibrary.wiley.com/terms-and-conditions) on Wiley Online Library for rules of use; OA articles are governed by the applicable Creative Commons License

minimize error propagation. For instance, users can plot the signal-to-noise ratio (SNR) during the LP signal processing step to choose the best sensors, frequencies, and time periods.

iFLOW supports comprehensive analysis of time series from multiple vertical sensors and provides tools for visualizing, processing, and adjusting intermediate results. Comparisons with synthetic numerical heat transport simulations show that iFLOW's models are well-implemented. Using a consistent framework and toolset, iFLOW offers guidelines for different methodologies. For example, FFT signal processing results improve with the detrending option and the Hanning windows function, which typically performs well under various noise conditions.

The performance of signal processing, but not of the model or parameter estimation technique, depends on sampling rate and window length. Our analysis shows that a window length of four times the dominant frequency period (4 P_d) of the top boundary temperature time series balances accuracy and temporal resolution for the forcing signal used here. For instance, a window length of 96 hr is a good first choice in natural streams where daily temperature fluctuations are often the dominant frequency and typical sampling resolution is 15 min. Higher temporal resolution may help signal processing with complex forcing signals. For the analyzed forcing signal, a 4 P_d window length does not require high-resolution sampling data. Shorter window lengths (1–2 P_d) need a 5-min sampling rate to minimize errors, but errors double for 2 P_d compared to 4 P_d. Disaggregating the original signal into smaller interpolated time steps may help by increasing the number of data points within the window, allowing for precise tracking of temporal changes in q, though this may introduce uncertainty in estimating q and k_e.

The LP-MLEn methodology, particularly the bounded domain model, provides robust solutions. The choice of reference sensor is crucial for defining noise within temperature signals. The performance of the local polynomial method depends on moving window length and sampling rate, impacting the number of data points available for phase and amplitude extraction, the SNR, and useable frequencies. For the selected forcing signal, data collection at 15-min intervals requires at least a 4 P_d moving window, while a 5-min sampling rate may allow for a 2 P_d window length in most cases. However, these guidelines depend on the quality of the collected temperature signals.

Overall, the LP-MLEn performs better than the other techniques studied here when a disturbance in the time-series occurs, for example, sudden change in interstitial velocity. This results in spikes of extracted signal amplitude, phase or quantified q and k_e that allow users to identify those values during data visualization and remove them in the estimated q and k_e. We recommend the use of LP-MLEn bounded when (a) more than three sensors are available, (b) they are continuously within the sediment, and (c) the sensor constraining the bottom condition has a SNR >5 dB. The LP-MLEn semi-infinite model is a valuable tool with two sensors and/or the low SNR (<5 dB) for the bottom sensor. However, LP-MLEn may be sensitive to changes in streambed elevation.

The deliberate choice of Python with open access and a modular framework allows users to add methods for data analysis, signal processing and parameter estimation, making it an ideal platform for further development, for example, for multi-dimensional heat transport analysis.

Data Availability Statement

The software (version 0.1.0) is licensed under GPL 3.0, including installer and source code. It is published on GitHub and accessible via Zenodo under the following link: https://doi.org/10.5281/zenodo.12708143. Data input are also available at Bertagnoli et al. (2024).

Video tutorials on how to use the software are available at iflowcode—YouTube (http://www.youtube.com/@iflowcode).

Acknowledgments

This research was partially supported by the Idaho Department of Water Resources (IDWR CON01285) and US Bureau of Reclamation (140R8120P0066). D.T. was partially supported by Hatch Act (Accession Number IDA01722) through the USDA National Institute of Food and Agriculture. DIFFER is part of the institute's organization of NWO. This work has been conducted within the framework of the EUROfusion Consortium, funded by the European Union via the Euratom Research and Training Programme (Grant Agreement No 101052200 — EUROfusion). Any opinions, conclusions, or recommendations expressed in this material are those of the authors and do not necessarily reflect the views of the supporting agencies. Neither the European Union nor the European Commission can be held responsible for them. Funding from the Royal Society (INF\R2\212060) for S.K. and the Leverhulme Trust (RPG-2021-030) for S. K. and U. S is also acknowledged.

References

Anibas, C., Fleckenstein, J. H., Volze, N., Buis, K., Verhoeven, R., Meire, P., & Batelaan, O. (2009). Transient or steady-state? Using vertical temperature profiles to quantify groundwater–surface water exchange. *Hydrological Processes*, *23*(15), 2165–2177. https://doi.org/10.1002/hyp.7289

Anibas, C., Schneidewind, U., Vandersteen, G., Joris, I., Seuntjens, P., & Batelaan, O. (2016). From streambed temperature measurements to spatial-temporal flux quantification: Using the LPML method to study groundwater-surface water interaction. *Hydrological Processes*, *30*(2), 203–216. https://doi.org/10.1002/hyp.10588

Anibas, C., Tolche, A. D., Ghysels, G., Nossent, J., Schneidewind, U., Huysmans, M., & Batelaan, O. (2018). Delineation of spatial-temporal patterns of groundwater/surface-water interaction along a river reach (Aa River, Belgium) with transient thermal modeling. *Hydrogeology Journal*, *26*(3), 819–835. https://doi.org/10.1007/s10040-017-1695-9

Barlow, J. R. B., & Coupe, R. H. (2009). Use of heat to estimate streambed fluxes during extreme hydrologic events. *Water Resources Research*, *45*(1). https://doi.org/10.1029/2007WR006121

Battin, T. J., & Sengschmitt, D. (1999). Linking sediment biofilms, hydrodynamics, and river bed clogging: Evidence from a large river. *Microbial Ecology*, *37*(3), 185–196. https://doi.org/10.1007/S002489900142

Baxter, C. V., & Hauer, F. R. (2000). Geomorphology, hyporheic exchange, and selection of spawning habitat by bull trout (Salvelinus confluentus). *Canadian Journal of Fisheries and Aquatic Sciences*, *57*(7), 1470–1481. https://doi.org/10.1139/f00-056

Bencala, K. E. (2005). Hyporheic exchange flows. In M. G. Anderson (Ed.), *Encyclopedia of hydrological Sciences*.

Bertagnoli, A., Luce, C., van Ricky, K., Schneidewind, U., Van Berkel, M., Tranmer, A. W., et al. (2024). iFLOW: A framework and GUI to quantify effective thermal diffusivity and advection in permeable materials from temperature time series (Version 1.0) [Software]. *Zenodo*. https://doi.org/10.5281/zenodo.12708143

Bianchin, M., Smith, L., & Beckie, R. (2010). Quantifying hyporheic exchange in a tidal river using temperature time series. *Water Resources Research*, *46*(7). https://doi.org/10.1029/2009WR008365

Boulton, A. J., Findlay, S., Marmonier, P., Stanley, E. H., & Valett, M. H. (1998). The functional significance of the hyporheic zone in streams and rivers. *Annual Review of Ecology and Systematics*, *29*(1), 59–81. https://doi.org/10.1146/annurev.ecolsys.29.1.59

Bredehoeft, J. D., & Papadopulos, I. S. (1965). Rates of vertical groundwater movement estimated from the Earth's thermal profile. *Water Resources Research*, *1*(2), 325–328. https://doi.org/10.1029/wr001i002p00325

Briggs, M. A., Lautz, L., McKenzie, J. M., Gordon, R. P., & Hare, D. (2012). Using high-resolution distributed temperature sensing to quantify spatial and temporal variability in vertical hyporheic flux. *Water Resources Research*, *48*(2), W02527. https://doi.org/10.1029/2011wr011227

Buss, S., Cai, Z., Cardenas, M. B., Fleckenstein, J. H., Hannah, D. M., Heppell, C. M., et al. (2011). *The hyporheic handbook A handbook on the groundwater – surface water interface and hyporheic zone for environment managers integrated catchment science programme science report: SC050070 the environment agency is the leading public body protecting and improving the environment in England and Wales*. UK Environmental Agency. Retrieved from https://assets.publishing.service.gov.uk/media/5a7cb90140f0b65b3de0ac46/scho1009brdx-e-e.pdf

Conant, B. J. (2004). Delineating and quantifying ground water discharge zones using streambed temperatures. *Ground Water*, *42*(2), 243–257. https://doi.org/10.1111/j.1745-6584.2004.tb02671.x

Conant, B. J., Cherry, J. A., & Gillham, R. W. (2004). A PCE groundwater plume discharging to a river: Influence of the streambed and near-river zone on contaminant distributions. *Journal of Contaminant Hydrology*, *73*(1–4), 249–279. https://doi.org/10.1016/j.jconhyd.2004.04.001

Constantz, J. (2008). Heat as a tracer to determine streambed water exchanges. *Water Resources Research*, *44*(4), W00D10. https://doi.org/10.1029/2008WR006996

Constantz, J., & Stonestorm, D. A. (2003). Heat as a tracer of water movement near streams. In D. A. Stonestorm & J. Constantz (Eds.), *Heat as a tool for studying the movement of ground water near streams*. US Geological Survey.

Constantz, J., & Thomas, C. L. (1996). The use of streambed temperature profiles to estimate the depth, duration, and rate of percolation beneath arroyos. *Water Resources Research*, *32*(12), 3597–3602. https://doi.org/10.1029/96wr03014

Cox, M. H., Su, G. W., & Constantz, J. (2007). Heat, chloride, and specific conductance as ground water tracers near streams. *Ground Water*, *45*(2), 187–195. https://doi.org/10.1111/j.1745-6584.2006.00276.x

DeWeese, T., Tonina, D., & Luce, C. (2017). Monitoring streambed scour/deposition under nonideal temperature signal and flood conditions. *Water Resources Research*, *53*(12), 10257–10273. https://doi.org/10.1002/2017WR020632

Ford, R. G., Lien, B. K., Acree, S. D., & Ross, R. R. (2021). Spreadsheet tools for quantifying seepage flux across the GW-SW interface. *Water Resources Research*, *57*(1), e2019WR026232. https://doi.org/10.1029/2019WR026232

Gordon, R. P., Lautz, L., Briggs, M. A., & McKenzie, J. M. (2012). Automated calculation of vertical pore-water flux from field temperature time series using the VFLUX method and computer program. *Journal of Hydrology*, *420–421*, 142–158. https://doi.org/10.1016/j.jhydrol.2011.11.053

Goto, S., Yamano, M., & Kinoshita, M. (2005). Thermal response of sediment with vertical fluid flow to periodic temperature variation at the surface. *Journal of Geophysical Research*, *110*(B1), B01106. https://doi.org/10.1029/2004jb003419

Hammett, S., Day-Lewis, F. D., Trottier, B., Barlow, P. M., Briggs, M. A., Delin, G., et al. (2022). GW/SW-MST: A groundwater/surface-WaterMethod selection too. *Ground Water*, *60*(6), 784–791. https://doi.org/10.1111/gwat.13194

Harris, F. J. (1978). On the use of windows for harmonic analysis with the discrete Fourier Transform. *Proceedings of the IEEE*, *66*(1), 51–83. https://doi.org/10.1109/PROC.1978.10837

Harvey, J. W., Drummond, J. D., Martin, R. L., McPhillips, L. E., Packman, A. I., Jerolmack, D. J., et al. (2012). Hydrogeomorphology of the hyporheic zone: Stream solute and fine particle interactions with a dynamic streambed. *Journal of Geophysical Research*, *117*(G4), G00N11. https://doi.org/10.1029/2012jg002043

Hatch, C., Fisher, A. T., Revenaugh, J. S., Constantz, J., & Ruehl, C. (2006). Quantifying surface water–groundwater interactions using time series analysis of streambed thermal records: Method development. *Water Resources Research*, *42*(10), W10410. https://doi.org/10.1029/2005wr004787

Irvine, D. J., Kurylyk, B. L., & Briggs, M. A. (2020). Quantitative guidance for efficient vertical flow measurements at the sediment–water interface using temperature–depth profiles. *Hydrological Processes*, *34*(3), 649–661. https://doi.org/10.1002/hyp.13614

Irvine, D. J., Lautz, L. K., Briggs, M. A., Gordon, R. P., & McKenzie, J. M. (2015). Experimental evaluation of the applicability of phase, amplitude, and combined methods to determine water flux and thermal diffusivity from temperature time series using VFLUX 2. *Journal of Hydrology*, *531*, 728–737. https://doi.org/10.1016/j.jhydrol.2015.10.054

Keery, J., Binley, A., Crook, N., & Smith, J. W. N. (2007). Temporal and spatial variability of groundwater–surface water fluxes: Development and application of an analytical method using temperature time series. *Journal of Hydrology*, *336*(1–2), 1–16. https://doi.org/10.1016/j.jhydrol.2006.12.003

Koch, F. W., Voytek, E. B., Day-Lewis, F. D., Healy, R., Briggs, M. A., Lane, J. W., & Werkema, D. (2016). *1DTempPro V2*: New Features for Inferring groundwater/surface-water exchange. *Ground Water*, *54*(3), 434–439. https://doi.org/10.1111/gwat.12369

Krause, S., Abbott, B. W., Baranov, V., Bernal, S., Blaen, P., Datry, T., et al. (2022). Organizational principles of hyporheic exchange flow and biogeochemical cycling in river networks across scales. *Water Resources Research*, *58*(3), 63–101. https://doi.org/10.1029/2021WR029771

Krause, S., Blume, T., & Cassidy, N. J. (2012). Investigating patterns and controls of groundwater up-welling in a lowland river by combining Fibre-optic Distributed Temperature Sensing with observations of vertical hydraulic gradients. *Hydrology and Earth System Sciences*, *16*(6), 1775–1792. https://doi.org/10.5194/hess-16-1775-2012

19447973, 2024, 11, Downloaded from https://agupubs.onlinelibrary.wiley.com/doi/10.1029/2024WR037370 by National Forest Service Library, Wiley Online Library on [28/02/2025]. See the Terms and Conditions (https://onlinelibrary.wiley.com/terms-and-conditions) on Wiley Online Library for rules of use; OA articles are governed by the applicable Creative Commons License

Lautz, L. (2012). Observing temporal patterns of vertical flux through streambed sediments using time-series analysis of temperature records. *Journal of Hydrology*, *464–565*, 199–215. https://doi.org/10.1016/j.jhydrol.2012.07.006

Lin, Y.-F., Chang, C.-H., & Tsai, J.-P. (2022). Analytical solution for estimating transient vertical groundwater flux from temperature-depth profiles. *Journal of Hydrology*, *610*, 127920. https://doi.org/10.1016/j.jhydrol.2022.127920

Luce, C. H., Tonina, D., Applebee, R., & DeWeese, T. (2017). Was that assumption necessary? Reconsidering boundary conditions for analytical solutions to estimate streambed fluxes. *Water Resources Research*, *53*(11), 9771–9790. https://doi.org/10.1002/2017wr020618

Luce, C., Tonina, D., & DeWeese, T. (2017). Data and numerical model for testing multifrequency analysis of temperature time series in streambeds [Dataset]. In *HydroShare Resources. HydroShare*. https://doi.org/10.4211/hs.cdd0ccc37c3b43179d63a4fcb2786c2d

Luce, C. H., Tonina, D., Gariglio, F., & Applebee, R. (2013). Solutions for the diurnally forced advection-diffusion equation to estimate bulk fluid velocity and diffusivity in streambeds from temperature time series. *Water Resources Research*, *49*(1), 488–506. https://doi.org/10.1029/2012WR012380

Marzadri, A., Dee, M. M., Tonina, D., Bellin, A., & Tank, J. L. (2014). A hydrologic model demonstrates nitrous oxide emissions depend on streambed morphology. *Geophysical Research Letters*, *41*(15), 5484–5491. https://doi.org/10.1002/2014GL060732

McAliley, W. A., Day-Lewis, F. D., Rey, D., Briggs, M. A., Shapiro, A. M., & Werkema, D. (2022). Application of recursive estimation to heat tracing for groundwater/surface-water exchange. *Water Resources Research*, *58*(6), e2021WR030443. https://doi.org/10.1029/2021WR030443

Mulholland, P. J., & DeAngelis, D. L. (2000). Surface-subsurface exchange and nutrient spiraling. In J. B. Jones & P. J. Mulholland (Eds.), *Streams and Ground Waters* (pp. 149–168). Academis Press.

Munz, M., & Schmidt, C. (2017). Estimation of vertical water fluxes from temperature time series by the inverse numerical computer program FLUX-BOT. *Hydrological Processes*, *31*(15), 2713–2724. https://doi.org/10.1002/hyp.11198

Pintelon, R., Schoukens, J., Vandersteen, G., & Barbé, K. (2010). Estimation of nonparametric noise and FRF models for multivariable systems—Part I: Theory. *Mechanical Systems and Signal Processing*, *24*(3), 573–595. https://doi.org/10.1016/j.ymssp.2009.08.009

Ren, J., & Packman, A. I. (2007). Changes in fine sediment size distributions due to interactions with streambed sediments. *Sedimentary Geology*, *202*(3), 529–537. https://doi.org/10.1016/j.sedgeo.2007.03.021

Rohling, H., & Schuermann, J. (1983). Discrete time window functions with arbitrarily low sidelobe level. *Signal Processing*, *5*(2), 127–138. https://doi.org/10.1016/0165-1684(83)90019-1

Rosenberry, D. O., Duque, C., & Lee, D. R. (2020). History and evolution of seepage meters for quantifying flow between groundwater and surface water: Part 1 – Freshwater settings. *Earth-Science Reviews*, *204*(March), 103167. https://doi.org/10.1016/j.earscirev.2020.103167

Schmidt, C., Büttner, O., Musolff, A., & Fleckenstein, J. H. (2014). A method for automated, daily, temperature-based vertical streambed water-fluxes. *Fundamental and Applied Limnology*, *184*(3), 173–181. https://doi.org/10.1127/1863-9135/2014/0548

Schneidewind, U., van Berkel, M., Anibas, C., Vandersteen, G., Schmidt, C., Joris, I., et al. (2016). LPMLE3: A novel 1-D approach to study water flow in streambeds using heat as a tracer. *Water Resources Research*, *52*(8), 6596–6610. https://doi.org/10.1002/2015wr017453

Schoukens, J., Rolain, Y., & Pintelon, R. (2005). Analysis of windowing/leakage effects in frequency response function measurements. *IFAC Proceedings Volumes*, *38*(1), IFAC–1160. https://doi.org/10.3182/20050703-6-cz-1902.00194

Shi, W., Wang, Q., Klepikova, M., Irvine, D. J., Rashed, A., & Liao, Z. (2024). Bdflux: A new bounded domain model for quantifying vertical fluxes in streambeds using heat as a tracer. *Journal of Hydrology*, *633*, 130981. https://doi.org/10.1016/j.jhydrol.2024.130981

Stallman, R. W. (1965). Steady 1 – Dimensional fluid flow in a semi-infinite porous medium with sinusoidal surface temperature. *Journal of Geophysical Research*, *70*(12), 282102827.

Stuart, T. A. (1954). Spawning sites of trout. *Nature*, *173*(4399), 354. https://doi.org/10.1038/173354a0

Swanson, T. E., & Cardenas, B. M. (2010). Ex-stream: A MATLAB® program for calculating fluid flux through sediment-water interfaces based on steady and transient temperature profiles. *Computers and Geosciences*, *37*(10), 1664–1669. https://doi.org/10.1016/j.cageo.2010.12.001

Tonina, D. (2012). Surface water and streambed sediment interaction: The hyporheic exchange. In C. Gualtieri & D. T. Mihailovic (Eds.), *Fluid mechanics of environmental interfaces* (pp. 255–294). CRC Press, Taylor and Francis Group.

Tonina, D., & Buffington, J. M. (2023). Physical and biogeochemical processes of hyporheic exchange in alluvial rivers. In F. Malard, C. Griebler, & S. Rétaux (Eds.), *Groundwater Ecology and Evolution* (pp. 61–87). Elsevier. https://doi.org/10.1016/B978-0-12-819119-4.15001-2

Tonina, D., Luce, C. H., & Gariglio, F. (2014). Quantifying streambed deposition and scour from stream and hyporheic water temperature time series. *Water Resources Research*, *50*(1), 287–292. https://doi.org/10.1002/2013WR014567

Vandersteen, G., Schneidewind, U., Anibas, C., Schmidt, C., Seuntjens, P., & Batelaan, O. (2015). Determining groundwater-surface water exchange from temperature-time series: Combining a local polynomial method with a maximum likelihood estimator. *Water Resources Research*, *51*(2), 922–939. https://doi.org/10.1002/2014wr015994

van Kampen, R., Schneidewind, U., Anibas, C., Bertagnoli, A., Tonina, D., Vandersteen, G., et al. (2022). LPMLE n –A frequency domain method to estimate vertical streambed fluxes and sediment thermal properties in semi-infinite and bounded domains. *Water Resources Research*, *58*(3), e2021WR030886. https://doi.org/10.1029/2021WR030886

Voytek, E. B., Drenkelfuss, A., Day-Lewis, F. D., Healy, R., Lane, J. W., & Werkema, D. (2014). 1DTempPro: Analyzing temperature profiles for groundwater/surface-water exchange. *Ground Water*, *52*(2), 298–302. https://doi.org/10.1111/gwat.12051

White, D. S., & Hendricks, S. P. (2000). Lotic macrophytes and surface-subsurface exchange processes. In J. B. Jones & P. J. Mulholland (Eds.), *Streams and ground waters* (pp. 363–379). Academic Press.

Woessner, W. W. (2020). *Groundwater-surface water exchange*. Groundwater Project.

Zarnetske, J. P., Gooseff, M. N., Bowden Morgan, J., Brosten, T. R., Bradford, J. H., & McNamara, J. P. (2008). Influence of morphology and permafrost dynamics on hyporheic exchange in arctic headwater streams under warming climate conditions. *Geophysical Research Letters*, *35*(L02501). https://doi.org/10.1029/2007gl032049

References From the Supporting Information

Rau, G. C., Cuthbert, M. O., McCallum, A. M., Halloran, L. J. S., & Andersen, M. S. (2015). Assessing the accuracy of 1-D analytical heat tracing for estimating near-surface sediment thermal diffusivity and water flux under transient conditions. *Journal of Geophysical Research: Earth Surface*, *120*, 1551–1573.

Reeves, J., & Hatch, C. E. (2016). Impacts of three-dimensional nonuniform flow on quantification of groundwater-surface water interactions using heat as a tracer. *Water Resources Research*, *52*(9), 6851–6866. https://doi.org/10.1002/2016WR018841

19447973, 2024, 11, Downloaded from https://agupubs.onlinelibrary.wiley.com/doi/10.1029/2024WR037370 by National Forest Service Library, Wiley Online Library on [28/02/2025]. See the Terms and Conditions (https://onlinelibrary.wiley.com/terms-and-conditions) on Wiley Online Library for rules of use; OA articles are governed by the applicable Creative Commons License